

# Studies of 19.5 GHz sky radiometric temperature: Measurements and applications

Shuen-Peng Shih and Yen-Hsyang Chu

Institute of Space Science, National Central University, Chung-Li, Taiwan

Received 20 December 2000; revised 2 November 2001; accepted 12 November 2001; published 8 May 2002.

[1] Using a single-frequency ground-based microwave radiometer with steerable horn antenna at frequency 19.5 GHz, we measure sky radiometric temperature over the Taiwan area during the period May 1997 to September 1999. Statistics indicate that for more than 80% of the time, in the absence of surface precipitation, the brightness temperature is above 27 K. Different elevation angle observations show that the median brightness temperature increases with decreasing elevation angle from about 30 K at zenith to about 128 K at 80° off-zenith angle. The opacity (or gaseous attenuation) is also estimated from measured brightness temperature. We found that the elevation angle variation of the median value of opacity follows exactly the secant law, while that of opacity with other probability does not. The mean radiated temperature  $T_m$  over the Taiwan area is also calculated using 5 years of radiosonde data, showing that  $T_m$  is a function of elevation angle and its value at 10° elevation angle is greater than that at zenith by 0.5–1.3%. A method of retrieving integrated precipitable water vapor content (IPWV) from the observed brightness temperature measured by a single-frequency radiometer at 19.5 GHz is developed and examined. Comparing the retrieved and measured IPWVs shows a good agreement between them, validating the method proposed in this article. The correlation between 19.5 GHz radiometric opacity and 52 MHz wind profiler backscatter from clear-air sky is also analyzed. The result shows that the correlation will be negative if the vertical distribution of the wind profiler backscatter is characterized by salient layered structures. Therefore great caution should be taken when radiometric measurements are incorporated with wind profiler backscatter to retrieve the humidity profile. *INDEX TERMS:* 3319 Meteorology and Atmospheric Dynamics: General circulation; 6904 Radio Science: Atmospheric propagation; 6952 Radio Science: Radar atmospheric physics; 6969 Radio Science: Remote sensing; *KEYWORDS:* microwave radiometer, brightness temperature, precipitable water vapor content, wind profiler, atmospheric attenuation

## 1. Introduction

[2] Radiometry is the measurement of electromagnetic radiation from an object with a certain temperature. A microwave radiometer is a highly sensitive receiver capable of measuring very low level microwave radiation from an object with temperature greater than absolute zero. Sometimes it is possible to establish a useful relation between the magnitude of the radiation intensity and a specific terrestrial or atmospheric parameter of interest. Once the relation is established, the desired parameter can thus be obtained from microwave radiometer measurements.

[3] The microwave radiometer has been proved to be an effective instrument in the remote sensing of atmosphere. Applications of the ground-based microwave radiometer

to measure meteorological parameters have been widely accepted in the community of atmospheric remote sensing for years [e.g., *Janssen*, 1993, and references therein]. Since the pioneering work of *Westwater* [1965], atmospheric temperature profiles were retrieved successfully by many scientists from radiometry measurements of gaseous emission using and applying various inversion techniques [*Snider*, 1972; *Westwater et al.*, 1975; *Decker et al.*, 1978; *Askne and Westwater*, 1982]. The accuracy of the radiometer-retrieved temperature, defined as the root-mean-square (RMS) difference between radiometer-measured and radiosonde temperatures, is generally less than 3 K [*Decker*, 1983]. The precipitable water vapor and cloud liquid can also be retrieved from the observations of a microwave radiometer operated at selected frequencies [*Guiraud et al.*, 1979; *Snider et al.*, 1980]. The retrieved accuracy of precipitable water vapor measured by the microwave radiometer is believed to be the same as or even better than those estimated by radiosonde

[Guiraud *et al.*, 1979]. In addition to the atmospheric temperature and precipitable water vapor, atmospheric attenuation of radio waves due to absorption of atmospheric gases, that is, water vapor and oxygen molecules, can also be estimated from the observed brightness temperature measured with a microwave radiometer. The atmospheric attenuation is an essential parameter in designing Earth-satellite communication links [Ippolito, 1986]. Westwater *et al.* [1990] measured the atmospheric attenuation using conversion of observed brightness temperatures at 20.6, 31.65, and 90 GHz and found that measurement and theory generally agree to within 30%. Microwave radiometric measurements may also be employed to estimate the propagation delay due to water vapor [Elgered, 1993]. Experimental results depict that the RMS error in measured wet delay using 19 and 22 GHz radiometers was about 1.5 cm [Moran and Rosen, 1981], which is significantly smaller than the 3.2 cm RMS error associated with the estimates based on surface meteorological parameters.

[4] Although the brightness temperature has been measured by many ground-based radiometers operated at various frequencies, to the authors' knowledge, the measurements at 19.5 GHz are not well documented. A portable ground-based 19.5 GHz radiometer was deployed alternately at Chung-Li (24.97°N, 121.19°E) and Tai-nan (22.94°N, 120.28°E) in Taiwan to monitor the sky noise temperature, or brightness temperature in compliance with the scientific mission of the satellite ROCSAT-1. The ROCSAT-1, launched successfully on 27 January 1999, is a low-Earth-orbit (LEO) scientific satellite orbiting at an altitude of about 600 km with an inclination of 35° and an orbital period of 97 min. One of the three scientific payloads mounted on the ROCSAT-1 is the Experimental Communication Payload (ECP) designed for Ka band communication experiments, in which a study of rain attenuation and scintillation effects on LEO satellite signal at Ka band, more specifically at 19.5 GHz, is included. In order to conduct the propagation experiment, besides the 19.5 GHz beacon transmitter on board and beacon receivers on the ground, a stand-alone ground-based 19.5 GHz radiometer in combination with a set of portable weather stations was employed to measure the background sky noise temperature. For more information on the details of ECP and the characteristics of the corresponding ground-based instruments, see Liu *et al.* [1999] and Shih and Chu [1999].

[5] In this article, the characteristics of 19.5 GHz brightness temperature observed in the period from 1997 to 1999 in the absence of surface precipitation are

presented and investigated, including long-term statistics, elevation angle dependence, behavior of corresponding opacity, and empirical relations between brightness temperature and other parameters. In light of the fact that mean radiating temperature  $T_m$  plays a key role in converting brightness temperature into atmospheric attenuation, the characteristics of  $T_m$  over the Taiwan area are also analyzed. We find that the mean value of  $T_m$ , varying in the range 270–298 K, is about 286 K over the Taiwan area, which is greater than the values reported in the literature [Wu, 1979]. This article is organized as follows: In section 2 we examine the characteristics of  $T_m$  over the Taiwan area, including elevation angle variation and a relation between  $T_m$  and surface temperature. The characteristics of brightness temperature at 19.5 GHz over the Taiwan area, including long-term statistics, elevation angle dependence, and linear relation between opacity (or equivalently, gaseous attenuation of atmosphere) converted from zenith brightness temperature and surface water vapor concentration, are presented and investigated in section 3. In section 4 we develop a method to retrieve the integrated precipitable water vapor content (IPWV) from zenith brightness temperature observed by a single-frequency radiometer at 19.5 GHz. With the help of radiosonde data an examination of the validity of the proposed method is also made in this section. A comparison between 19.5 GHz radiometric temperature and 52 MHz wind profiler backscatter is made in section 5, and conclusions are given in section 6.

## 2. Effective Radiated Temperature

[6] Effective radiated (or weighted mean) temperature  $T_m$  is one of the essential parameters in deducing atmospheric opacity (or atmospheric attenuation)  $\tau_0(\theta)$  from observed brightness temperature  $T_b$  in accordance with the following expression [Ulaby *et al.*, 1981; Ingold *et al.*, 1998]:

$$\tau_0(\theta) = 4.34 \ln \left[ \frac{T_c - T_m}{T_b(\theta) - T_m} \right] \text{ dB}, \quad (1)$$

where  $T_b(\theta)$  is the brightness temperature,  $\theta$  is the elevation angle, and  $T_c$  is the cosmic noise temperature (approximately equal to 2.7 K).  $T_m$  is defined as

$$T_m = \frac{\int_0^\infty T_e(z) \alpha_a(z) e^{-\tau(z,\theta)} dz}{\int_0^\infty \alpha_a(z) e^{-\tau(z,\theta)} dz}, \quad (2)$$

where  $\alpha_a$  as a function of height is the gaseous absorption coefficient in units of decibels (or nepers)

**Table 1.** Regression Coefficients for Different Regressive Lines  $Y = a + bX$ 

$Y$	$X$	$a$	$b$	$c^a$
$T_m$ (K)	$T_s$ (K)	28.84	0.87	0.96
$d_m$ (cm)	$T_b$ (K)	-3.373	0.755	0.91
$\tau_0$ (dB)	$\rho_0$ (g m <sup>-3</sup> )	0.2816	0.0194	0.76

<sup>a</sup>Here,  $c$  is correlation coefficient.

per kilometer,  $T_e$  is the thermometric temperature of the atmospheric gaseous, and  $\tau(z, \theta)$  is the opacity of the atmosphere at height  $z$  and elevation angle  $\theta$ . It should be noted that under the condition of spherical symmetry for  $\theta < 75^\circ$ ,  $\tau(z, \theta)$  can be well approximated to  $\tau(z)\sec(\theta)$  with error less than 1% and  $\tau(z)$  can be defined as  $\tau(z) = \int_0^z \alpha_a(z) dz$ . It is well acknowledged that the tropospheric temperature decreases linearly with height at lapse rate  $\gamma$  and can be described by

$$T(z) = T_s + \gamma z, \quad (3)$$

where  $T_s$  is surface temperature. Substituting equation (3) into equation (2) yields

$$T_m = T_s + \gamma F(\theta), \quad (4)$$

where

$$F(\theta) = \frac{\int_0^\infty z e^{-\chi(z,\theta)} d\chi}{1 - e^{-\tau_0(\theta)}} \quad (5)$$

and  $\chi(z, \theta) = \tau(z, \theta)$ . Using radiosonde data taken at the Pan-Chiao station in the period January 1994 to September 1999, the characteristics of  $F(\theta)$  are analyzed. International Telecommunication Union Radiocommunication Sector (ITU-R) gaseous absorption coefficients are employed in equation (5) to calculate  $F(\theta)$  [ITU, 1997]. Calculation shows that  $F(\theta)$  decreases monotonically with the increase of elevation angle and the magnitude of  $F(0^\circ)$  varies from 0.8 to 2.52 with a mean value of 1.7 and is greater than that of  $F(50^\circ)$  by 2%, and greater than that of  $F(80^\circ)$  by about 15%. From equation (4), one would expect that theoretically,  $T_m$  is linearly dependent on  $T_s$  with the proportionality constant of 1. The regressive line connecting zenith effective radiating temperature  $T_{mz}$  (corresponding to the condition of  $\theta = 0^\circ$ ) and  $T_s$  is obtained by best fitting linear equation  $T_{mz} = a + bT_s$  to the observed data during the period from January 1994 to September 1999. The estimated regression coefficients are shown in Table 1. Our result indicates that  $T_{mz}$  over the Taiwan area varies in the range of about 270–298 K with a mean value of 286 K. The

estimated slope of the regression line is about 0.874. Presumably, the discrepancy between the estimated slope and the theoretical one is attributed to the statistical fluctuations and/or the assumption of linear variation of temperature with height.

### 3. Brightness Temperature

[7] In this section, the characteristics of the brightness temperature  $T_b$  and the atmospheric opacity (or attenuation) measured by a 19.5 GHz radiometer over the Taiwan area are presented, including long-term statistics and zenith variation. The application of zenith  $T_b$  to the retrieval of integrated precipitable water vapor will be discussed in section 4.

#### 3.1. Facility

[8] A portable microwave radiometer with steerable horn antenna is employed for the measurement of brightness temperature in this study. This ground-based radiometer is a single linearly polarized, superheterodyne, and Dicke-switched instrument. The central frequency of the radiometer is 19.5 GHz with IF bandwidth of 500 MHz. The half power beam width of the horn antenna is approximately  $6^\circ$ , and the sensitivity is 0.5 K for an integration time of 1 s. The linearly polarized radiation, either horizontal or vertical, is selected by orienting the feed horn vertically or horizontally. The voltage signal from the radiometer is fed into the low-pass filter/amplifier that determines the integration time of the radiometer. The low-pass filter used for the measurements has a various cutoff frequency for integration times between 4 and 1024 ms. The horizontal or vertical signal from the low-pass filter is sent to a printer/recorder for viewing the data in real time and to a data collection board connected to the bus of the host personal computer that controls the data acquisition. The data collection board digitizes the radiometer output with 12 bit precision. The positions of the antenna in azimuth and elevation are recorded at each time when the radiometer signals are sampled. The detailed characteristics of the 19.5 GHz radiometer are summarized in Table 2.

[9] In reality, the noise temperature measured by a radiometer contains not only true sky noise temperature but also system noise temperature. Therefore proper calibration of the radiometer is required to derive constants for use in the radiometer equation to estimate the absolute sky noise temperature. The 19.5 GHz radiometer employed in this experiment has a Dicke reference load and an avalanche noise diode that serves as an internal calibration source. In addition to the

**Table 2.** Characteristics of Microwave Radiometer

Parameter	Specification
Central frequency/polarization	19.5 GHz/single linear
Input bandwidth	1 GHz
IF bandwidth	500 MHz
Antenna	conical feed horn
Half power beam width of horn antenna	6°
Noise figure	
Mixer-preamplifier	4.0 dB
Isolator	0.3 dB
Filter	0.2 dB
Latching circulator	0.3 dB
Waveguide	0.2 dB
Total	5.0 dB
Integration time	4–1024 ms
Input range	0–313 K
Sensitivity	0.5–1 K
Accuracy	1–2 K
Switch rate	2.2 KHz
Dynamic range	0–350 K
Receiver type	superheterodyne, double-sideband, noise injection Dicke type
Size	30" <i>L</i> × 18" <i>W</i> × 12" <i>H</i>
Weight	25 lb
Power supply	120 V, 60 Hz, 5 A maximum

internal calibration the radiometer is also calibrated using external loads before the deployment of the field experiment. The hot and cold calibrations are performed in this experiment by using 0°C (273 K) ice water and −196°C (77 K) liquid nitrogen, respectively. These two points permit an absolute calibration of the radiometer.

### 3.2. Observations

[10] The observations of brightness temperatures were carried out using a steerable and transportable 19.5 GHz radiometer over the period from May 1997 to September 1999 at Chung-Li and Tai-nan separately. Two modes of the experiments were performed alternately. One mode is the continuous measurement of zenith brightness temperatures by steering the horn antenna of the radiometer vertically. The data collected in this way were employed to calculate the long-term statistics of the zenith brightness temperature. The other mode is the measurement of elevation angle variation of the brightness temperature by steering the horn antenna from zenith to 10° elevation angle at a step of 10°. The azimuth angle was kept constant during the measurement. The dwelling time of the measurement at each zenith angle is 10 min. There are 88 cases in total for the multiangle observation of

brightness temperature performed at Chung-Li (42 cases) and Tai-nan (46 cases) within these 2 years.

[11] Figures 1a and 1b present the statistics of the zenith variations of brightness temperatures recorded at Chung-Li and Tai-nan, respectively. As expected, the brightness temperature, observed at either Chung-Li or Tai-nan, increases monotonically with the elevation angle. The median brightness temperature at 10° elevation angle for the Chung-Li site is greater than that at zenith by a factor of 4.3, being 4.2 for the Tai-nan site. Employing equation (2), the opacity can be estimated from the measured brightness temperature. We find that the median value of opacity exactly follows the secant law as shown in Figures 1a and 1b, where a bold solid curve in each plot represents the realization of  $\sec(\theta)$ . However, the ratios for opacities with other probabilities do not follow the secant law. Moreover, 98% of brightness temperatures at 10° elevation angle for the Chung-Li and Tai-nan sites are in the range of 72–200 K and 110–190 K, respectively. In addition, no matter what the zenith angle is, the brightness temperatures at Tai-nan are generally greater than those at Chung-Li. This is because, on average, the surface humidity at Tai-nan (located in the southern part of Taiwan) is usually greater than that at Chung-Li (located in the northern part of Taiwan) by a factor of 1.2. Moreover, the variation range of brightness temperature at Chung-Li is larger than that at Tai-nan, implying that the change in the humidity for Chung-Li is larger than that for Tai-nan. These long-term statistical results imply that the background atmospheric noise environment at Ka band over the Taiwan area is characterized by large median value and highly fluctuating brightness temperature. Figure 2b presents the cumulative distributions of zenith brightness temperature recorded at Chung-Li in the absence of surface precipitation. We used 60,500 data points with 1 min average. The median value of brightness temperature is 33 K, and 80% of the brightness temperatures occur in the range from 24 K to 39 K. Figure 2a shows the cumulative distribution of wet delay calculated from the data taken from the Pan-Chiao radiosonde station for the period from January 1994 to September 1999. Long-term statistics demonstrates that the wet delay over the Taiwan area varies in the range from 5 cm to 40 cm with the mean value of 23 cm. Figure 3 depicts the seasonal variation of wet delay, showing that the maximum occurs in the summer and the minimum is in the wintertime. The difference of averaged wet delay between summer and winter is about 13 cm.

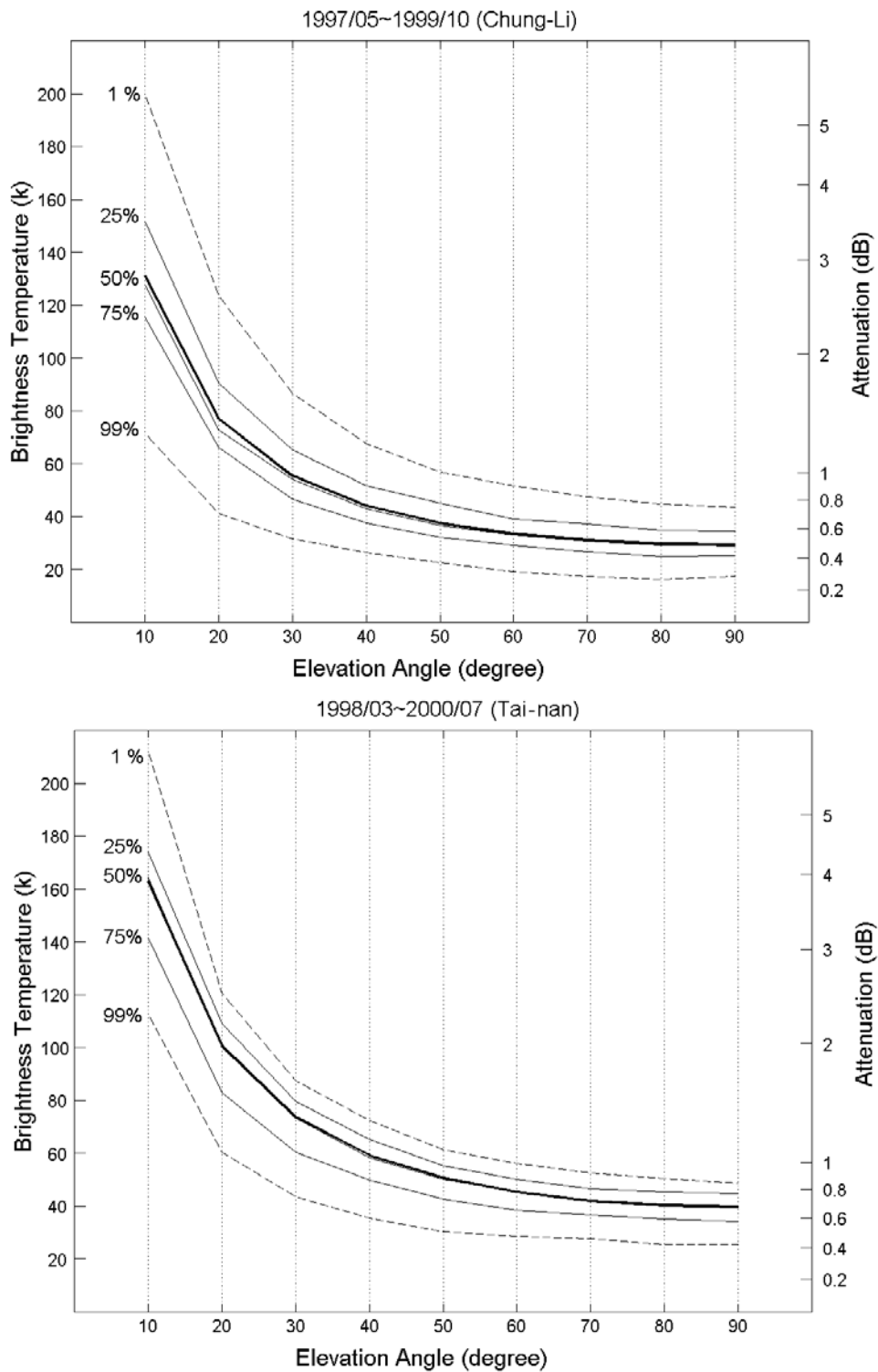


**Figure 1.** Long-term statistics of zenith variation of brightness temperature measured at the (a) Chung-Li site and (b) Tai-nan site. Note that the bold curve in each panel is the realization of  $\tau_0 \sec(\theta)$ , where  $\theta$  is zenith angle and  $\tau_0$  is attenuation at zenith.



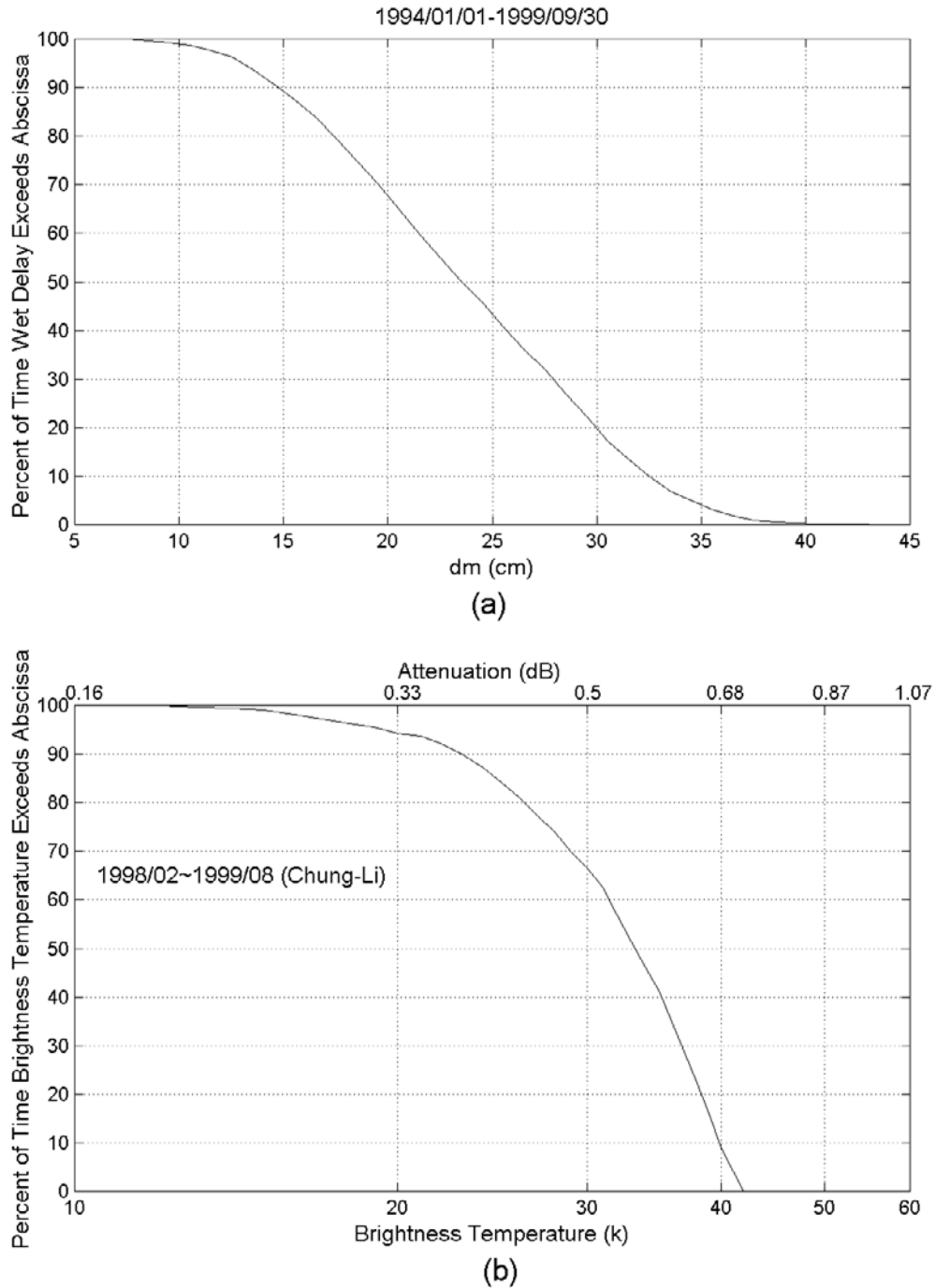


**Figure 2.** (a) Cumulative distribution of wet delay calculated from meteorological data taken at the Pan-Chiao radiosonde station from January 1994 to September 1999. (b) Cumulative distribution of zenith brightness temperature recorded at the Chung-Li site for the period from February 1998 to August 1999.

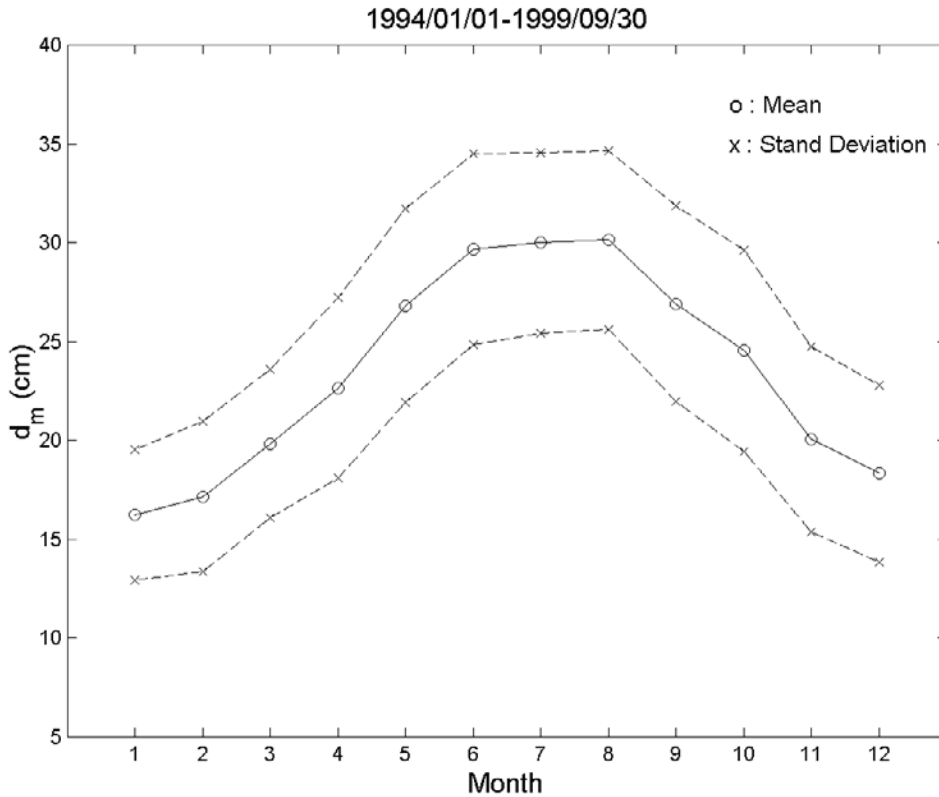


Figure 3. Seasonal variation of wet delay over Taiwan area.

[12] As mentioned above, the observed radiation intensity measured by a 19.5 GHz radiometer is highly sensitive to the emission of water vapor. As a result, it is expected that the observed brightness temperature will be strongly correlated to the wet delay calculated from the radiosonde data. The empirical relation between wet delay and zenith brightness temperature at 19.5 GHz in the absence of surface precipitation over the Taiwan area is analyzed, and the result is presented in Table 1. As indicated, the correlation between wet delay and zenith brightness temperature is significantly high, about 0.95. The regression line between them is obtained as  $d_m = -3.373 + 0.755T_{bz}$ , where the units of  $d_m$  and  $T_{bz}$  are centimeters and kelvins, respectively. The number of cases employed for the statistical analysis is 133 in total. A detailed examination reveals that the RMS error of observed  $d_m$  deviating from the regressive line is about 3 cm, comparable to that associated with the estimates based on surface meteorological parameters [Moran and Rosen, 1981].

[13] The relation between zenith opacity measured by various ground-based radiometers operated at different

frequencies and the surface water vapor density is reported in the literature [e.g., Ulaby *et al.*, 1981]. However, this relation is not well documented at the frequency of 19.5 GHz. The linear regression relation between zenith opacity  $\tau_o$  at 19.5 GHz and surface water vapor density  $\rho_o$  is obtained by best fitting regression line  $\tau_o = a + b\rho_o$  to the observed data, and the result is shown in Table 1, in which the units of  $\tau_o$  and  $\rho_o$  are decibels and  $\text{g cm}^{-3}$ , respectively.

#### 4. Retrieval of Integrated Precipitable Water Vapor

[14] According to the radiative transfer theory the brightness temperature measured by a ground-based microwave radiometer is the integration of the radiation emitted by the absorptive gases in the antenna beam. Once the brightness temperatures are measured, the corresponding total atmospheric attenuation due to gas absorption can be converted directly in accordance with equation (1). Alternatively, the gas attenuation can be calculated in accordance with  $\int_0^z \alpha_a(z) dz$  if the profile of

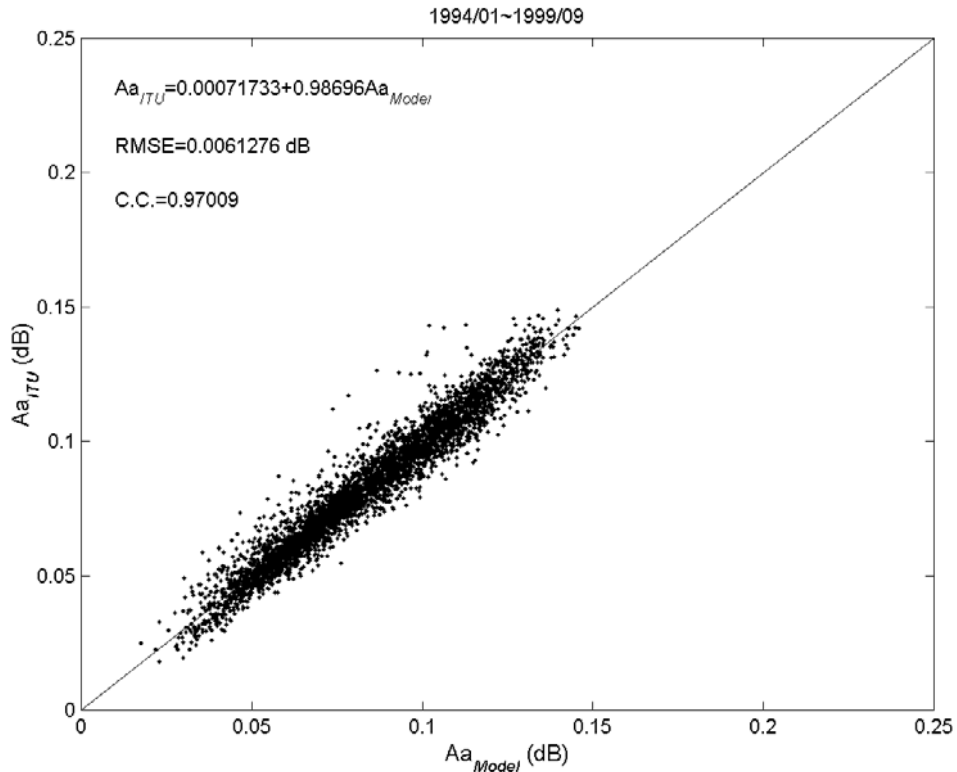


**Figure 4.** Comparison between gaseous attenuations calculated by approximation equation (6) and ITU-recommended equation. RMSE, root-mean-square error; c.c., correlation coefficient.

specific attenuation coefficient  $\alpha_a$  as a function of absorbing gas concentrations is given. Although oxygen molecules and water vapor both give rise to radio wave absorption, computation shows that in the Taiwan area the contribution of water vapor to the absorption is much more significant than that of oxygen molecules by a factor of about 12, where the meteorological data employed for the calculation are taken from the Pan-Chiao rawinsonde station over the period from 1 August 1994 to 30 November 1999. This result implies that oxygen absorption can be reasonably neglected in retrieving water vapor content from radiometer-observed brightness temperature.

[15] Ideally, the radiometer-measured attenuation should be identical to the calculated one if the expression of the specific attenuation coefficient is accurate enough and the total amount of water vapor content responsible for the measured and calculated attenuations is the same. Therefore, with the help of a relevant approximation equation connecting the gaseous absorption and water vapor concentration, it is possible to estimate the integrated precipitable water vapor content

(IPWV) from the brightness temperature measured by a single-frequency ground-based radiometer. An approximation equation as a complicated function of temperature, pressure, and water vapor concentration has been recommended by ITU to calculate the gas attenuation. However, the ITU-recommended equation is too complicated for use in retrieving water vapor content from the measurements of a single-frequency radiometer. The purpose of this section is to find a more simple, but accurate enough, approximation equation to estimate IPWV from the gas attenuation observed by a single-frequency ground-based microwave radiometer. By appropriately adjusting the constants in the ITU-recommended approximation equation [ITU, 1997] a very simple approximation expression at the frequency of 19.5 GHz is proposed as follows:

$$\alpha_w = 0.00036 + 2.14 \times 10^{-3} \rho_w \quad \text{dB km}^{-1}, \quad (6)$$

where  $\rho_w$  is the water vapor concentration in units of  $\text{g m}^{-3}$ . An examination of the accuracy of the approximation equation as shown in equation (6) is made, and the results



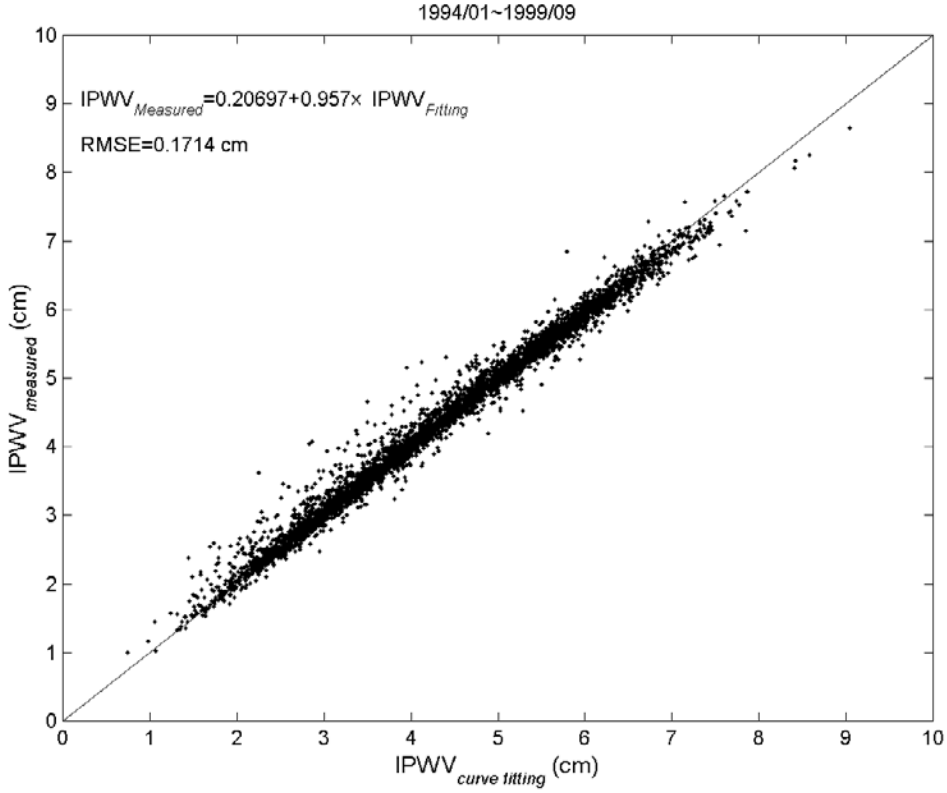


**Figure 5.** Comparison between integrated precipitable water vapor IPWV estimated from the measured profile of water vapor density and calculated by best fitting the exponential model to the measured profile.

are presented in Figure 4, where 69 months radiosonde data from 1 January 1994 to 30 September 1999 are employed for the examination. As indicated, the attenuations  $A_a$  calculated from the approximation equation agree very well with those estimated from the ITU-recommended equation with RMS of less than 0.0061. This good agreement validates the usefulness of equation (6). Note that  $A_a$  is defined as

$$A_a = \int_0^{r_o} \alpha_w(z) dz \quad \text{dB}, \quad (7)$$

where  $r_o$  is the maximum height that the water vapor extends up to and can be detected by the radiosonde. Assume that the concentration of water vapor decreases with height exponentially in the form of

$$\rho_w = \rho_{ws} \exp\left(-\frac{z}{H_w}\right) \quad \text{g m}^{-3}, \quad (8)$$

where  $\rho_{ws}$  and  $H_w$  are surface concentration ( $\text{g m}^{-3}$ ) and scale height (kilometers) of water vapor concentration, respectively. Note that the integrated precipitable water

vapor content (IPWV)  $h_v$  can be estimated in accordance with following equation:

$$h_v = \frac{M_v}{10\rho_L} = \frac{\int_0^{r_o} \rho_w dz}{10\rho_L} \quad \text{cm}, \quad (9)$$

where  $\rho_L$  is the density of liquid water (equal to approximately  $1 \text{ g cm}^{-3}$ ),  $\rho_w$  is the water vapor concentration (in units of  $\text{g m}^{-3}$ ),  $r_o$  (in units of kilometers) is the highest altitude that the radiosonde can reach, and  $M_v$  ( $\text{g km m}^{-3}$ ) is the total mass of atmospheric water vapor contained in a vertical column of unity cross section. It is obvious that in practice the measured profile of  $\rho_w$  may not necessarily decrease with height exponentially. However, data analysis indicates that  $h_v$  estimated from the real profile of  $\rho_w$  recorded by radiosonde is very close to that calculated using the exponential model, as shown in Figure 5. Therefore it is justified to estimate  $h_v$  in terms of the exponentially decreasing model. Substituting equation (8) into equations (6) and (7), we have

$$A_a = Br_o + C\rho_{ws}H_w\left(1 - e^{-r_o/H_w}\right) \quad \text{dB}, \quad (10)$$

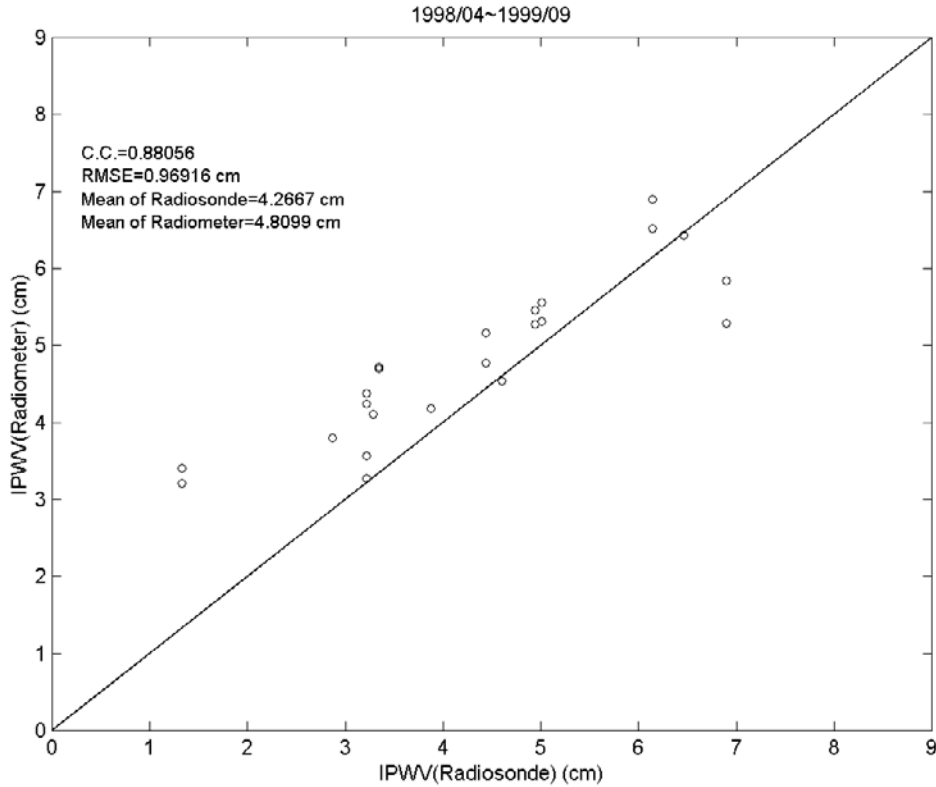


**Figure 6.** Comparison of IPWVs estimated from radiosonde data and retrieved from zenith opacity measured by a 19.5 GHz radiometer.

where  $B = 0.00036 \text{ dB km}^{-1}$  and  $C = 2.14 \times 10^{-3} \text{ dB m}^3 \text{ g}^{-1} \text{ km}^{-1}$ . From equations (9) and (10) the IPWV  $h_v$  can thus be derived as follows:

$$h_v = \frac{A_a - Br_o}{10C\rho_L(1 - e^{-r_o/H_w})} \text{ cm.} \quad (11)$$

Note that the mean values of  $r_o$  and  $H_w$  over the Taiwan area are 10 and 2.2 km, respectively, producing that  $Br_o = 0.0036 \text{ dB}$  and  $\exp(-r_o/H_w) \sim 0.0106$ . In view of the fact that  $A_a$  is, in general, greater than  $Br_o$  by 1–2 orders of magnitude and  $1 - \exp(-r_o/H_w) \sim 0.99$ ,  $Br_o$  and  $\exp(-r_o/H_w)$  can reasonably be neglected in the use of equation (11) to calculate IPWV from observed zenith opacity  $\tau_o$  by letting  $\tau_o$  be equal to  $A_a$  as defined in equation (7). Figure 6 presents the comparison of IPWVs estimated from radiosonde data and retrieved from zenith gaseous attenuation observed by a 19.5 GHz radiometer, where the data employed for the comparison are collected under clear-air conditions to avoid the effects of both cloud and precipitation on observed brightness temperature. As shown, the retrieved IPWVs are in good agreement with the measured ones, with RMS error of

about 0.97 cm. Note that the Pan-Chiao rawinsonde station is located about 25 km northeast from the Chung-Li station. It is reasonable to speculate that the water vapor contents over Pan-Chiao and Chung-Li will be different because of spatial inhomogeneity. We believe that this is the major cause of the few points with large scatter. Therefore the method of retrieving IPWV from the measurements of a single-frequency radiometer proposed in this section is applicable.

## 5. Comparison Between 19.5 GHz Atmospheric Attenuation and 50 MHz Wind Profiler Backscatter

[16] As mentioned in section 4, the brightness temperature at 19.5 GHz results primarily from the radiation of water vapor, and therefore the atmospheric attenuation  $A_a$  due to water vapor absorption (as defined in equation (7)) is directly proportional to the total amount of water vapor content in a column of atmosphere. Because the mathematical relationship between atmospheric attenuation and water vapor is well established, microwave

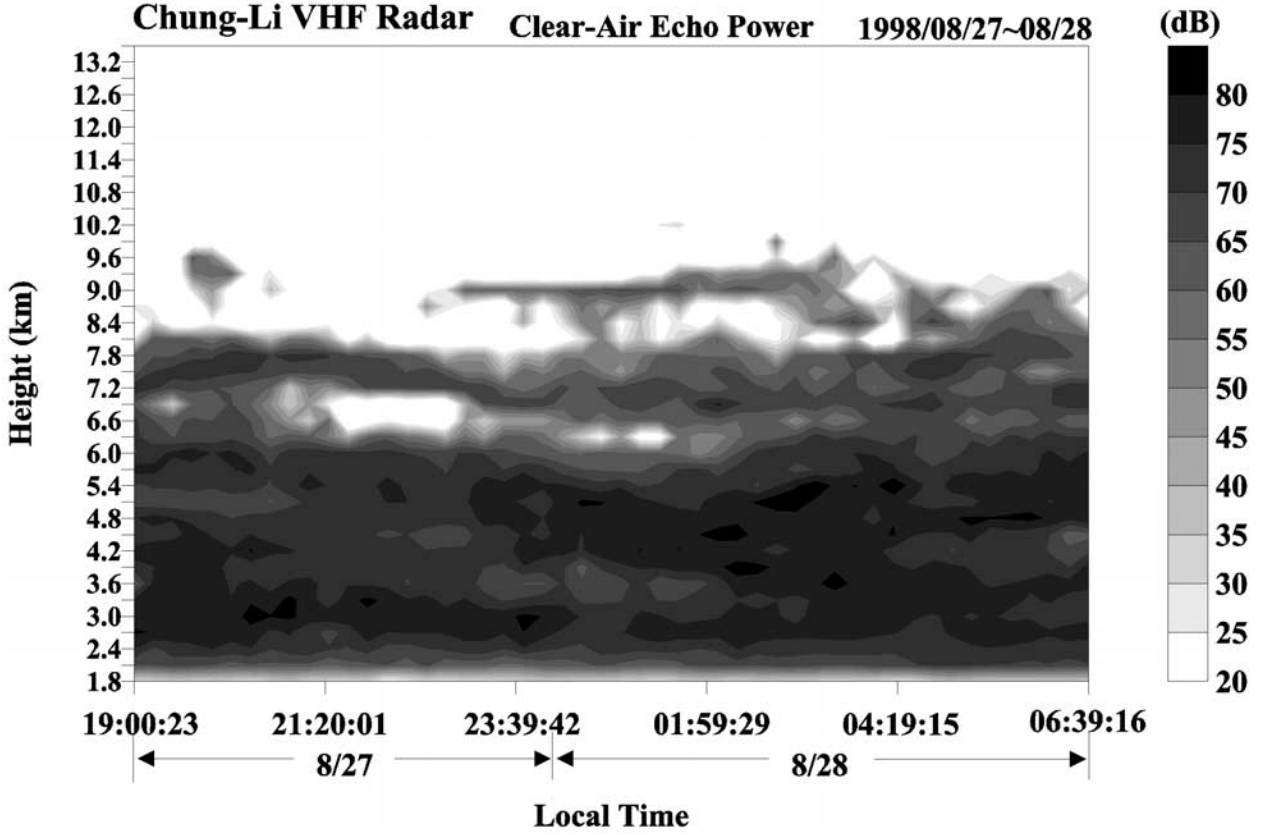


Figure 7. Height-time-intensity plot for clear-air echo power measured by the Chung-Li VHF radar at 52 MHz.

radiometric data have been employed not only to estimate the total amount of water vapor but also to retrieve the water vapor profile, also incorporating measurements obtained from other instruments [Skoog *et al.*, 1982]. Wind profiler backscatter generated from turbulence-induced refractivity fluctuations was also considered to be able to provide usable information to improve the accuracy of humidity profile retrieval [Stankov *et al.*, 1996]. An attempt is made in this section to examine the relation between radiometer-measured opacity and 50 MHz wind profiler backscatter. Theoretical and experimental results both show that wind profiler backscatter is strongly correlated to the gradient of the potential refractive index, the so-called  $M$  parameter, defined as follows [Ottersten, 1969]:

$$M = \frac{dn}{dz} = -77.6 \times 10^{-6} \left( \frac{P}{T} \right) \left( \frac{\partial \ln \Theta}{\partial z} \right) \cdot \left[ 1 + 15500 \frac{q}{T} \left( 1 - \frac{1}{2} \frac{\frac{\partial \ln q}{\partial z}}{\frac{\partial \ln \Theta}{\partial z}} \right) \right], \quad (12)$$

where  $n$  is potential refractive index,  $T$  is temperature (kelvins),  $P$  is pressure (hPa),  $\Theta$  is potential temperature (kelvins), and  $q$  is specific humidity. In order to compare  $M$  and  $A_d$  the relation between  $M$  and water vapor density  $\rho_w$  should be established. In light of the fact that water vapor density  $\rho_w$  is generally smaller than dry air density  $\rho_d$  by 2 orders of magnitude, specific humidity can be thought to be very close to mixing ratio [Wallace and Hobbs, 1977]. Substituting  $q \cong \rho_w R_d T / P$  and  $\Theta = T (P_r / P)^{R_d / c_p}$  into equation (12), where  $P_r$  is atmospheric pressure at reference altitude and  $c_p$  is specific heat at constant volume, equation (12) reduces to

$$M = GR_d \left( C_1 \rho_d + C_2 \rho_w + C_3 \frac{d\rho_w}{dz} \right), \quad (13)$$

$$C_1 = \frac{d \ln T}{dz} - 0.286 \frac{d \ln P}{dz},$$

$$C_2 = \frac{15500}{2T} \left( \frac{d \ln T}{dz} + 0.428 \frac{d \ln P}{dz} \right),$$

$$C_3 = -\frac{15500}{2T},$$

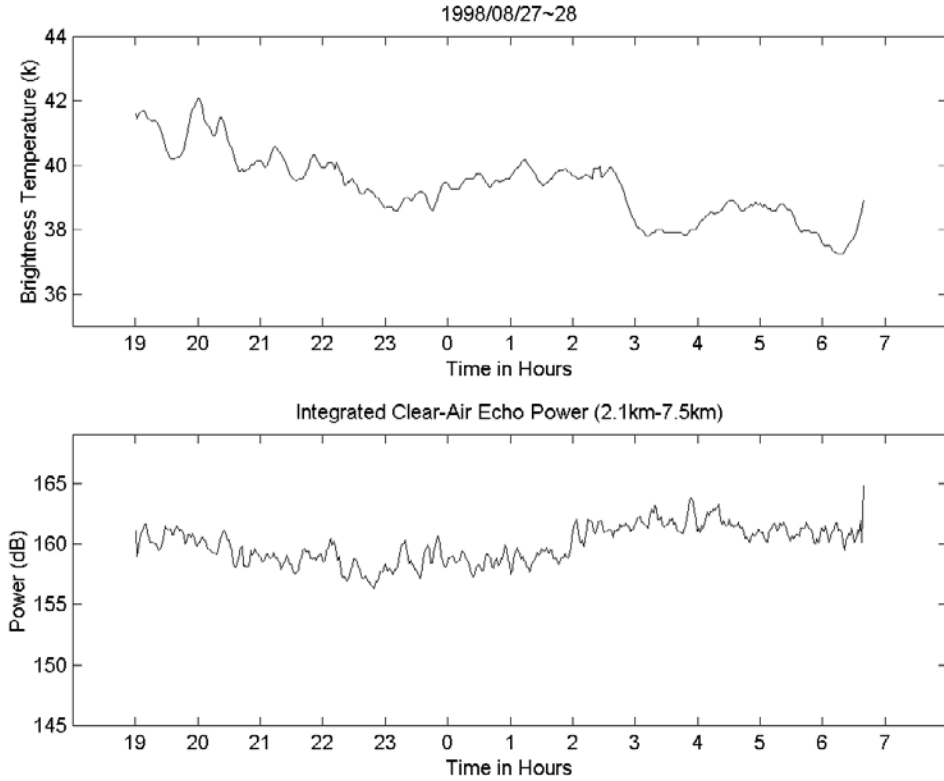


**Figure 8.** Comparison between 19.5 GHz brightness temperature and integrated backscatter at 50 MHz under clear-air sky conditions. The 50 MHz radar beam and 19.5 GHz radiometric horn antenna are both pointed vertically.

where  $G = -77.6 \times 10^{-6}$ ,  $R_d$  is the dry gas constant ( $287 \text{ J deg}^{-1} \text{ kg}^{-1}$ ), and  $R_d/c_p = 0.286$ . The magnitudes of  $C_1$ ,  $C_2$ , and  $C_3$  can be estimated as follows: Assume that  $P = P_o \exp(-z/H_p)$  and  $T = T_o - \gamma z$ , where  $P_o$  is pressure at surface,  $H_p$  is scale height, and  $\gamma$  is temperature lapse rate. As a result,  $C_1 = 0.286/H_p - \gamma/T$  and  $C_2 = 155,000(\gamma/T + 0.428/H_p)/2T$ . Note that in the lower and middle troposphere,  $\gamma \sim 0.006-0.008 \text{ deg m}^{-1}$ ,  $H_p \sim 8000 \text{ m}$ ,  $T \sim 265-300 \text{ K}$ ,  $\rho_d \sim 1.275 \text{ kg m}^{-3}$ , and  $\rho_w \sim 0.009-0.012 \text{ kg m}^{-3}$  [Wallace and Hobbs, 1977]. In addition, in situ measurements made with a radiosonde show that it is not uncommon that  $d\rho_w/dz \sim 10^{-5}-10^{-6} \text{ kg m}^{-4}$  [Luce et al., 1995; Vaughan and Worthington, 2000]. Therefore we have  $C_1\rho_d \sim 10^{-5}-10^{-6}$ ,  $C_2\rho_w \sim 3 \times 10^{-5}$  to  $3 \times 10^{-6}$ , and  $C_3 d\rho_w/dz \sim 10^{-4}-10^{-5}$ . Obviously, for an environment with high humidity, the dry term  $C_1\rho_d$  in equation (13) will be smaller than the other two wet terms by 1–2 orders of magnitude and can be ignored. This is especially true for the environment in Taiwan. Taiwan is a small island located in a subtropical region. Its atmosphere is characterized by warm temperature and high humidity.

Statistics shows that during the summer season the vertical extent to which humidity contributes to wind profiler backscatter cannot be ignored, since it can be as high as 8 km [Chu et al., 1990]. Define integrated  $M$  parameter  $M_I$  as follows:

$$M_I = \int M dz = GR_d \left( \int C_2 \rho_w dz + \int C_3 \frac{d\rho_w}{dz} dz \right). \quad (14)$$

It is expected that  $M_I$  is proportional to the height-integrated square root of VHF backscattered power. If  $\rho_w$  and  $d\rho_w/dz$  are random processes, the correlation function between  $M_I$  and  $A_a$  can be expressed as follows:

$$\langle A_a M_I \rangle = GR_d \left( \iint C_2 \langle \rho_{w1} \rho_{w2} \rangle dz_1 dz_2 + \iint C_3 \left\langle \frac{d\rho_{w1}}{dz} \rho_{w2} \right\rangle dz_1 dz_2 \right), \quad (15)$$

where the angle brackets represent an ensemble average. If we assume further that the processes of  $\rho_w$  (and  $d\rho_w/dz$ ) at

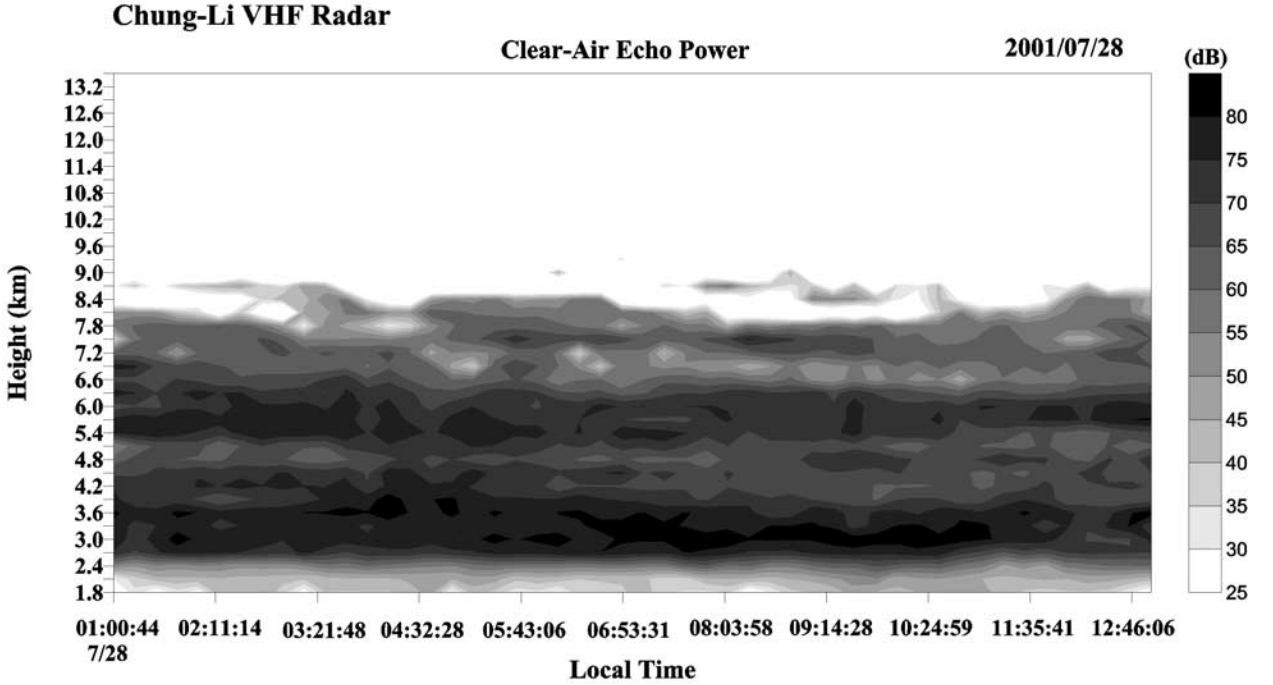


Figure 9. Same as Figure 7, but the data were taken on 28 July 2001, 0100–1246 LT.

different altitudes are independent and uncorrelated to each other, equation (15) reduces to

$$\langle A_a M_I \rangle = GR_d z_0 \left( \int C_2 U_{\rho\rho} dz + \int C_3 V_{\rho\rho'} dz \right), \quad (16)$$

where  $U_{\rho\rho}$  and  $V_{\rho\rho'}$  are an autocorrelation function of  $\rho_w$  and a correlation function of  $\rho_w$  and  $d\rho_w/dz$ , respectively, and  $z_0$  is the height extent of data coverage in the vertical. Obviously, the correlation between the height-integrated square root of VHF backscattered power and radiometer-measured atmospheric attenuation is determined by height integration of  $U_{\rho\rho}$  and  $V_{\rho\rho'}$ . For an environment with uniform distribution of  $\rho_w$  in the vertical (that is,  $d\rho_w/dz=0$ ) a positive correlation is expected between  $A_a$  and  $M_I$ . However, a negative correlation between  $A_a$  and  $M_I$  is likely to occur if  $d\rho_w/dz$  is remarkable and negatively correlates to  $\rho_w$ . In fact, the radar experiment conducted with the Chung-Li VHF radar indeed exhibited varying correlations between integrated VHF backscattered power and radiometer-measured atmospheric attenuation. Figure 7 is the height-time-intensity plot of backscattered power observed using the 52 MHz Chung-Li VHF radar under clear-air sky conditions during the period from 28 August 1998, 1900 LT, to 28 August 1998, 0639 LT. Figure 8 compares the time series of integrated VHF radar

echo power and atmospheric attenuation measured by the 19.5 GHz radiometer. The Chung-Li VHF radar is a wind profiler located on the campus of National Central University in Taiwan. The antennas of the radiometer and the Chung-Li VHF radar were both steered vertically. The radar parameters employed for the experiment are as follows: interpulse period, 500  $\mu$ s; pulse length, 2  $\mu$ s; coherent integration time of the radar returns, 30 ms; and number of range gates used, 40. A 128-point fast Fourier transform algorithm was used to calculate a raw Doppler spectrum. After 10 times of incoherent integration of the raw spectra the echo power was calculated from the resulting Doppler spectrum, and noise power was removed in the calculation. The echo powers were integrated in the height range 2.1–7.2 km as presented in Figure 7 to produce the radar data shown in Figure 8. At a first glance at Figure 8 it appears that there is no consistent relation between atmospheric attenuation and 52 MHz radar backscatter. However, inspecting the time series in more detail indicates that a significant positive correlation between the two is seen for the data before 0000 LT on 28 August, while a negative correlation is seen for the data after that time. Calculation shows that the coefficients of the correlations between atmospheric attenuation and height-integrated square root of the wind profiler backscattered power for the data before and after

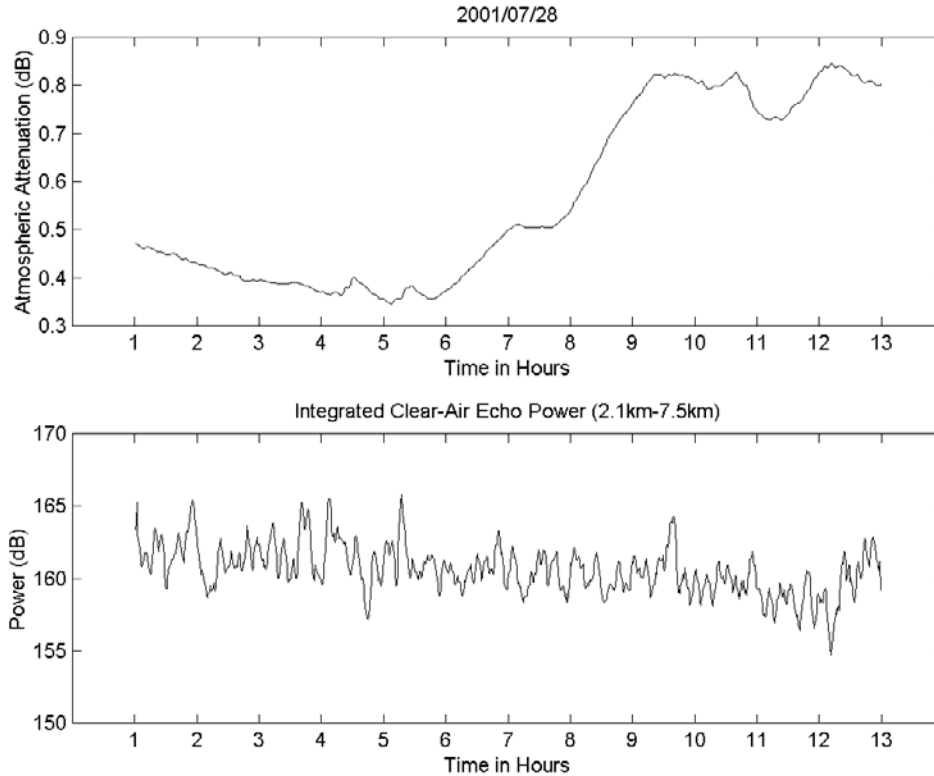


**Figure 10.** Same as Figure 8, but the data were taken on 28 July 2001, 0100–1246 LT.

0000 LT are 0.64 and  $-0.52$ , respectively. Inspecting the vertical distribution of VHF radar echo power shown in Figure 7 in more detail indicates that the layered structure of the echo power after 0000 LT is much more pronounced than that before 0000 LT. From equation (13) we note that vertical gradient of water vapor density dominates the magnitude of  $M$ . Moreover, theoretical investigations and radar experiments both show that VHF backscatter from atmospheric refractivity fluctuations is proportional to  $M^2$  [Gage and Balsley, 1980; Tsuda *et al.*, 1988; Chu *et al.*, 1990]. Therefore it is reasonable to speculate that the layered structures characterized by intense backscatter as shown in Figure 7 are very likely associated with the vertical gradient of water vapor density, leading to a negative correlation between radiometric measurement and height-integrated wind profiler backscatter, as expected in accordance with equation (16). Figure 9 shows another example of a height-time-intensity plot of VHF backscatter with pronounced layered structures taken by the Chung-Li VHF radar on 27 July 2001, 0100–1246 LT. In analogy to the data of 28 August from 0000 LT to 0639 LT shown in Figure 7, the correlation between radiometric measurements and integrated VHF

backscatter for the data shown in Figure 9 is also negative, with a coefficient of  $-0.489$ , and their time series are shown in Figure 10. Therefore correlation between radiometric measurement and wind profiler backscatter seems to be a plausible indicator in the qualitative assessment of the significance of the vertical structure of humidity. However, more data are required to validate this speculation.

## 6. Conclusion

[17] The characteristics of 19.5 GHz brightness temperature over the Taiwan area measured by a ground-based radiometer in the absence of surface precipitation are presented and investigated in this article. Multiangle observations show that the brightness temperature increases with the zenith angle from 18–42 K at zenith to 70–200 K at  $10^\circ$  elevation angle. Long-term statistics indicates that for more than 80% of the time the zenith brightness temperature is above 30 K over the Taiwan area. We attribute the feature of high brightness temperature to high water vapor content over the Taiwan area. The dependence of opacity (or gaseous attenuation) on



zenith angle is also studied. Basically, the median value of opacity follows perfectly the secant law, while opacities with other probabilities do not. With the help of the ITU-recommended equation a method of retrieving integrated precipitable water vapor content using zenith opacity measured by a single-frequency radiometer at 19.5 GHz is developed in this article. A comparison of retrieved IPWV and observed IPWV measured with the radiosonde shows good agreement between them, validating the proposed method. A comparison between 19.5 GHz radiometric measurement and 52 MHz wind profiler backscatter is also made in this article. The result shows that the correlation in the two is highly variable and dominated by the height variation of water vapor concentration. Therefore great caution should be taken when radiometric measurements are incorporated with wind profiler backscatter for retrieval of the humidity profile.

[18] **Acknowledgments.** This work was supported by the National Space Program Office of Taiwan under grants NSC89-NSPO-A-ECP-008-01 and NSC89-2111-M-008-029-A10.

## References

- Askne, J., and E. R. Westwater, A review of ground-based remote sensing of temperature and moisture by passive microwave radiometers, *IEEE Trans. Geosci. Remote Sens.*, *GE-24*, 340–352, 1982.
- Chu, Y. H., C. H. Liu, J. Rottger, T. S. Hsu, L. H. Chen, and J. K. Chao, A study of the characteristics of VHF radar echo power in the Taiwan area, *Radio Sci.*, *25*, 527–538, 1990.
- Decker, M. T., A comparison of radiosonde- and radiometrically-derived atmospheric observations, paper presented at Fifth Symposium on Meteorological Observations and Instrumentation, Am. Meteorol. Soc., Toronto, Ont., Canada, 1983.
- Decker, M. T., E. R. Westwater, and F. O. Guiraud, Experimental evaluation of ground-based microwave radiometric sensing of atmospheric temperature and water vapor profiles, *J. Appl. Meteorol.*, *17*, 1788–1795, 1978.
- Elgered, G., Tropospheric radio-path delay from ground-based microwave radiometry, in *Atmospheric Remote Sensing by Microwave Radiometry*, edited by M. A. Janssen, pp. 215–258, John Wiley, New York, 1993.
- Gage, K. S., and B. B. Balsley, On the scattering and reflection mechanisms contributing to clear-air radar echoes from the troposphere, stratosphere, and mesosphere, *Radio Sci.*, *15*, 243–257, 1980.
- Guiraud, F. O., J. Howard, and D. C. Hogg, A dual-channel microwave radiometer for measurement of precipitable water vapor and liquid, *IEEE Trans. Geosci. Electron.*, *GE-17*, 129–136, 1979.
- Ingold, T., R. Peter, and N. Kampfer, Weighted mean tropospheric temperature and transmittance determination at millimeter-wave frequencies for ground-based applications, *Radio Sci.*, *33*, 905–918, 1998.
- International Telecommunication Union (ITU), Attenuation by atmospheric gases, *Recomm. ITU-R P.676-3*, Geneva, 1997.
- Ippolito, L. J., Jr., *Radiowave Propagation in Satellite Communication*, 241 pp., Van Nostrand Reinhold, New York, 1986.
- Janssen, M., *Atmospheric Remote Sensing by Microwave Radiometry*, 572 pp., John Wiley, New York, 1993.
- Liu, G. S., S. J. Yu, J. K. Ho, J. Lin, and P. Chen, Experimental communication payload project of the ROCSAT-1 satellite, *TAO, suppl.*, 127–144, 1999.
- Luce, H., M. Crochet, F. Dalaudier, and C. Sidi, Interpretation of VHF ST radar vertical echoes from in situ temperature sheet observations, *Radio Sci.*, *30*, 1003–1025, 1995.
- Moran, J. M., and B. R. Rosen, Estimation of the propagation delay through the troposphere from microwave radiometer data, *Radio Sci.*, *16*, 235–244, 1981.
- Ottersten, H., Atmospheric structure and radar backscattering in clear air, *Radio Sci.*, *4*, 1179–1193, 1969.
- Shih, S. P., and Y. H. Chu, Ka band propagation experiments of experimental communication payload (ECP) on ROCSAT-1: Preliminary results, *TAO, suppl.*, 145–164, 1999.
- Skoog, B. G., J. I. Askne, and G. Elgered, Experimental determination of water vapor profiles from ground-based radiometer measurements at 21.0 and 31.4 GHz, *J. Appl. Meteorol.*, *21*, 394–400, 1982.
- Snider, J. B., Ground-based sensing of temperature profiles from angular and multi-spectral microwave emission measurements, *J. Appl. Meteorol.*, *11*, 958–967, 1972.
- Snider, J. B., F. O. Guiraud, and D. C. Hogg, Comparison of cloud liquid content measurement by two independent ground-based systems, *J. Appl. Meteorol.*, *19*, 577–579, 1980.
- Stankov, B. B., E. R. Westwater, and E. E. Gossard, Use of wind profiler estimations of significant moisture gradients to improve humidity profile retrieval, *J. Atmos. Oceanic Technol.*, *13*, 1285–1290, 1996.
- Tsuda, T., P. T. May, T. Sato, S. Kato, and S. Fukao, Simultaneous observations of reflection echoes and refractive index gradient in the troposphere and lower stratosphere, *Radio Sci.*, *23*, 655–665, 1988.
- Ulaby, F. T., R. K. Moore, and A. K. Fung, *Microwave Remote Sensing: Active and Passive*, vol. 1, 456 pp., Addison-Wesley-Longman, Reading, Mass., 1981.
- Van Vleck, J. H., and V. F. Weisskopf, On the shape of collision broadened lines, *Rev. Mod. Phys.*, *17*, 227–236, 1945.
- Vaughan, G., and R. M. Worthington, Effects of humidity and precipitation on VHF radar vertical beam echoes, *Radio Sci.*, *35*, 1389–1398, 2000.
- Wallace, J. M., and P. V. Hobbs, *Atmospheric Science: An Introductory Survey*, 467 pp., Academic, San Diego, Calif., 1977.
- Westwater, E. R., Ground-based passive probing using the mi-

- crowave spectrum of oxygen, *J. Res. Natl. Bur. Stand., Sect. D*, 69, 1201–1211, 1965.
- Westwater, E. R., J. B. Snider, and A. V. Carlson, Experimental determination of temperature profiles by ground-based microwave radiometry, *J. Appl. Meteorol.*, 14, 524–539, 1975.
- Westwater, E. R., J. B. Snider, and M. J. Falls, Ground-based radiometric observations of atmospheric emission and attenuation at 20.6, 31.65, and 90.0 GHz: A comparison of measurements and theory, *IEEE Trans. Antennas Propag.*, 38, 1569–1580, 1990.
- Wu, S. C., Optimum frequencies of a passive microwave radiometer for tropospheric path-length correction, *IEEE Trans. Antennas Propag.*, 27, 233–239, 1979.
- 
- Y.-H. Chu and S.-P. Shih, Center for Space and Remote Sensing Research, Institute of Space Science, National Central University, Chung-Li 32054, Taiwan. (yhchu@jupiter.ss.ncu.edu.tw)